High-*Q* Dynamic Force Microscopy in Liquid and Its Application to Living Cells

J. Tamayo,* A. D. L. Humphris,† R. J. Owen,† and M. J. Miles†
*Instituto de Microelectrónica de Madrid (CSIC), 28760 Tres Cantos, Madrid, Spain; and †H. H. Wills Physics Laboratory, University of Bristol, Bristol BS8 1TL, United Kingdom

ABSTRACT We present a new dynamic force microscopy technique for imaging in liquids in the piconewton regime. The low quality factor (*Q*) of the cantilever is increased up to three orders of magnitude by the implementation of a positive feedback control. The technique also includes a phase-locked loop unit to track the resonance of the cantilever. Experiments and computer simulations indicate that the tip-sample forces are below 100 pN, about two orders of magnitude lower than in conventional tapping mode atomic force microscopy. Furthermore, the spectroscopic ability is greatly enhanced. Either the phase shift or the resonant frequency shows a high sensitivity to variations in either the energy dissipation or conservative interactions between the tip and the sample, respectively. The potential of this technique is demonstrated by imaging living cells.

INTRODUCTION

Since the invention of atomic force microscopy (AFM) in 1986 (Binnig et al., 1986), the topography of inorganic and organic materials has been visualized at the nanometer scale (Rugar and Hansma, 1990; Bustamante and Keller, 1995). The achievement of higher resolution (i.e., atomic or molecular spatial resolution), has required novel developments. The implementation of dynamic force microscopy (DFM) has been crucial, providing true atomic resolution of inorganic surfaces in ultra-high vacuum (Giessibl, 1995; Sugurawa et al., 1995). In DFM, the cantilever oscillation is monitored instead of the deflection (DC-AFM), so changes in the amplitude, phase, or resonance due to the tip-sample interaction are measured. This detection method has shown a sensitivity four orders of magnitude higher than that in DC-AFM in detecting long-range attractive forces (Martin et al., 1987).

Visualization of biological material has greatly benefited from the development of the DFM techniques (Bustamante and Keller, 1995; Shao et al., 1996; Kasas et al., 1997). First, these samples are soft and are significantly deformed by the nanonewton-regime forces applied in DC-AFM. Second, these materials adhere weakly to the substrate and can easily be displaced or destroyed by the lateral forces that arise during the scanning of the tip in contact with the sample. Moreover, imaging in physiological solution is crucial for the study of the native structure and function of the biomolecules. The invention of tapping mode (TM AFM) has allowed the visualization of delicate samples in air; in this DFM technique the tip makes intermittent contact with the surface of the sample, minimizing the destructive lateral forces (Zhong et al., 1993). This technique was immediately used for imaging in liquid environments, now being one of the most widespread AFM techniques for the characterization of biomolecules (Hansma et al., 1994; Putman et al., 1994).

The oscillation of a cantilever in a liquid presents important differences compared with oscillation in air or ultra-high vacuum (Butt et al., 1993; Chen et al., 1994a). First, the cantilever motion drags the surrounding liquid, leading to an increase of the effective mass by a factor of 10-40 and a corresponding decrease of the resonant frequency. Second, the strong hydrodynamic interaction between the cantilever and the liquid produces a very low quality factor (Q) of ~2-10, about two orders of magnitude lower than in air. Both effects have profound consequences on the cantilever oscillation in the intermittent contact regime (Tamayo, 1999). The cantilever oscillation is anharmonic and asymmetric when the quality factor is low, in contrast with TM AFM in air, where the cantilever oscillation is approximately sinusoidal and symmetric (Chen et al., 1994b; Cleveland et al., 1998; Tamayo and García, 1996).

The low quality factor of the cantilever in a liquid implies high forces between the tip and the sample. This can be explained by describing the experimental situation in dynamic force microscopy as a nanooscillator (cantilever) in a nonlinear potential (tip-sample interaction) (Fig. 1 *A*). This system can be approximated as two springs in series; one is the cantilever with a spring constant k_c, and the other represents the tip-sample force with a spring constant k_{ts}, equal to the force gradient (Fig. 1 *B*). Thus, the effective spring constant of the cantilever changes ($k_c' = k_c - k_{ts}$), and the resonance shifts from f_0 to $f_0' = f_0(1 - k_{ts}/k_c)^{1/2}$. In DFM in liquid, the tip-sample interaction is detected via damping of the amplitude at a fixed frequency, so the resonance shift owing to the interaction produces an amplitude damping at resonance, which is proportional to the quality factor of the cantilever (Fig. 1, *C* and *D*). The insensitivity of the cantilever in a liquid implies high forces of several nanonewtons that can produce a high deformation

Received for publication 3 August 2000 and in final form 27 March 2001.
Address reprint requests to Dr. Javier Tamayo, Centro Nacional de Microelectronica, Isaac Newton 8 (Parque de Madrid), Tres Cantos, Spain. Tel.: 34-91-8060700; Fax: 34-91-8060701; E-mail: jtamayo@imm.cnm.csic.es.

0006-3495/01/07/526/12 $2.00

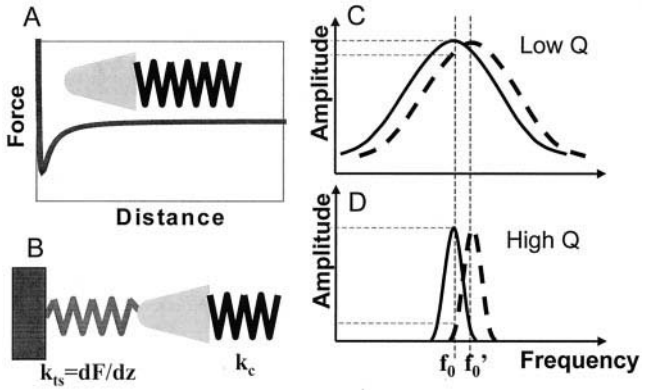

FIGURE 1 (*A*) Scheme of the experimental situation in dynamic force microscopy represented as a nanooscillator (cantilever) in a nonlinear force field (tip-sample interaction). In (*B*) the tip-sample interaction is approximated as a spring of constant k_{ts} equal to the gradient force. (*C*) and (*D*) show the amplitude fall at resonance as a consequence of resonance shift due to the tip-sample interaction for a cantilever with low and high *Q* value, respectively.

and damage in biological specimens (Tamayo et al., 2000). These forces are at least an order of magnitude greater than those used to obtain molecular resolution of proteins in solution using DC-AFM (~100 pN). This perhaps could explain why DC-AFM has obtained the best resolution so far for biomolecules in solution (Engel et al., 1999; Shao et al., 1996). However, these results have been obtained in 2-D crystals of proteins whose roughness is of a few angstroms. Also, keeping the deflection signal to a very low force in DC-AFM is technically difficult as a consequence of the thermal drift (~100 pN/min). Dynamic force microscopy is insensitive to the thermal drift and does not produce lateral forces that can disrupt the rough samples.

Here we present a novel DFM technique for liquids in which the cantilever response is controlled by adding an active feedback system that increases the quality factor up to three orders of magnitude. This technique allows imaging of soft materials with a force of ~10 pN in TM AFM in liquids, at least two orders of magnitude smaller than the forces in the conventional technique (Tamayo et al., 2000). Furthermore, this technique allows decoupling of the tip-sample interaction into its elastic and dissipative components. This has been applied to single molecule force spectroscopy to study the mechanical properties of dextran (Humphris et al., 2000). In this work, the features of this technique are described in detail. First the experimental set-up and cantilever response are described, then the interaction between the tip and the sample are studied experimentally and by the use of numerical simulations. In the Spectroscopy section we discuss the spectroscopic aspect of this technique, in which it is possible to measure either the amplitude and the phase of the cantilever oscillation or the resonant frequency and amplitude at resonance. In this section analytical expressions are provided to determine the energy dissipated between the tip and the sample. Finally, the potential of this technique is demonstrated with images of living cells.

MATERIALS AND METHODS

A commercial atomic force microscope (Nanoscope IIIa with Multi Mode head, Veeco Digital Instruments) with a liquid cell was used with either magnetic or acoustic excitation. To enable magnetic excitation (Han et al., 1996; Lantz et al., 1999) a coil was wound into a recess in the fluid cell normally used to retain a rubber o-ring. Both methods used silicon nitride cantilevers with a nominal spring constant of 0.37 N/m. Cantilevers for driving with the magnetic field were modified by coating with chromium and then cobalt using thermal evaporation. A magnetic moment was induced in the thin film with a strongly oriented magnetic field. The oscillation amplitude used was typically 10 nm with resonant frequencies of 12.5-17.0 kHz.

To theoretically calculate the force, sample deformation, and contact time between the tip and the sample in TM AFM, the second-order differential equation of a driven damped harmonic oscillator in a nonlinear potential was solved numerically (Tamayo and García, 1996):

$$m\frac{d^2z}{dt^2} + \gamma\frac{dz}{dt} + kz = F_0\cos(\omega t) + F_{\text{int}}(z) \qquad (1)$$

where m is the effective mass of the lever, γ is the damping constant, k is the spring constant, $F_0\cos(\omega t)$ is the driving force, and $F_{\text{int}}(z)$ is the tip-sample force at a tip-sample separation z. The resonant frequency of the cantilever is $\omega_0 = (k/m)^{1/2}$ and the quality factor is $Q = m\omega_0/\gamma$. The interaction between the tip and the sample $F_{\text{int}}(z)$ consists of a repulsive force during the contact between the tip and the sample that takes into account the mechanical properties of the sample. This repulsive force is modeled by the Hertz model, in which the tip and the sample are approximated by a paraboloid and a flat surface, respectively (Israelachvili, 1992). For simplicity, van der Waals forces and electrostatic forces have not been included in these calculations, as this does not alter the conclusions of this work. The numerical calculations were programmed in Fortran; the main routines of the program consist of a fourth-order Runger-Kutta routine with adapted step size to solve the differential equation numerically, and a fast Fourier transform routine that provides the frequency spectrum of the cantilever motion.

The differential equation of the cantilever motion when the positive feedback control is introduced in the experimental set-up to increase the quality factor has an additional driving force proportional to the main harmonic of the motion ($A_1\cos(\omega t - \varphi)$) shifted 90°:

$$m\frac{d^2z}{dt^2} + \gamma\frac{dz}{dt} + kz = F_0\cos(\omega t) + GA_1\cos(\omega t - \varphi + \pi/2) + F_{\text{int}}(z) \qquad (2)$$

The numerical solution of this equation uses a conditional loop that compares A_1 and φ with the amplitude and phase shift of the first harmonic of the solution of Eq. 2. The loop is completed when the solution exhibits a deviation in amplitude and phase of <0.01 nm and 0.01°, respectively.

Normal rat kidney cells were grown at 37°C and 5% carbon dioxide in Dulbecco's modified Eagles medium containing 10% heat-inactivated fetal calf serum, 100 μg/ml streptomycin, and 100 μg/ml penicillin. The cells were grown directly onto uncoated glass coverslips and were washed in PBS (phosphate buffered saline, pH 7.4) before being imaged in a small amount of fresh growth medium at room temperature. To analyze the details of the cell structure, phase shift images of the living cells were treated with a contrast enhancement routine in Fig. 9, *C* and *D*. This routine runs a statistical differencing filter on the image, bringing all the features

of the image to the same height by subtracting the mean height of small regions of the image. Here it was performed for regions of 32 × 32 pixels in images acquired with a resolution of 512 × 512 pixels.

DESCRIPTION OF THE TECHNIQUE

Cantilever motion in DFM

In conventional dynamic force microscopy, the cantilever response (z) to the incident forces (F) can be expressed as $z(\omega) = \chi(\omega)F(\omega)$, in which the cantilever transfer function (χ) can be approximated as that of a damped harmonic oscillator:

$$\chi(\omega) = \frac{{\omega_0}^2/k}{{\omega_0}^2 - \omega^2 + i\omega_0\omega/Q} \tag{3}$$

where ω_0 and ω are, respectively, the resonant and incident force frequencies, k is the spring constant of the cantilever, and Q is the quality factor.

The forces acting on the cantilever are the driving force that excites the cantilever $F_{ext} = F_0 e^{i\omega t}$, the thermal force and the interaction force between the tip and the sample (F_{int}). During the cantilever oscillation, the interaction depends on time as the tip-sample distance is $z \approx z_0 + Ae^{i\omega t}$.

$$\begin{aligned} F_{int}(z) &= F_{int}(z_0) + \frac{dF_{int}}{dz}(z_0)\Delta z + \frac{1}{2}\frac{d^2F_{int}}{dz^2}(z_0)\Delta z^2 + \cdots \\ &= F_{int\,0} + F_{int\,1}e^{i\omega t} + F_{int\,2}e^{i2\omega t} + \cdots = F_{int}(t) \end{aligned} \tag{4}$$

Neglecting the thermal force, the total force acting on the cantilever is:

$$\begin{aligned} F_{tot} &= F_{int\,0} + (F_0 + F_{int\,1})e^{i\omega t} + F_{int\,2}e^{i2\omega t} + \cdots \\ &\equiv F_{int\,0} + F_1(\omega) + F_2(2\omega) + \cdots \end{aligned} \tag{5}$$

which produces a cantilever response $z = \chi(\omega)F_{tot}$,

$$\begin{aligned} z &= z_0 + A_1 e^{i(\omega t - \varphi_1)} + A_2 e^{i(2\omega t - \varphi_2)} + \cdots \\ &\equiv z_0 + z_1(\omega) + z_2(2\omega) + \cdots \end{aligned} \tag{6}$$

Equations 5 and 6 allow explaining the Q-dependence of the cantilever motion in DFM. Indeed, the cantilever motion is sinusoidal in air and vacuum, but it is anharmonic in liquid with a significant contribution of higher harmonics (Tamayo, 1999). When the driving frequency is close to resonance ($\omega \approx \omega_0$), the contribution of the higher harmonics of the interaction force, $F_n(n\omega_0)$ ($n > 1$), to the cantilever motion, $z_n(n\omega_0)$ is more significant as the resonance peak is broader, i.e., lower Q. Thus, the ratio between the cantilever responses to the second harmonic and first harmonic components of the force is $\mathrm{mod}(\chi(2\omega_0)/\chi(\omega_0)) \approx 2/3\ 1/Q$, explaining why the cantilever motion in DFM in air is sinusoidal ($Q = 50 - 500$), but it has an important contribution of higher harmonic in liquid ($Q \sim 1$).

Cantilever motion control

The cantilever response is not necessarily restricted by the physical conditions. Cantilever motion control can change the cantilever response to that of a cantilever in an environment with different viscosity, temperature, etc. The general principle is shown in Fig. 2 *A*. This set-up introduces a controller that feeds back the cantilever motion with a defined transfer function $C(\omega)$ to the driving force unit (Mertz et al., 1993; Garbini et al., 1996; Durig et al., 1997; Anczykowski et al., 1998). Hence the cantilever response $\chi(\omega)$ is modified, giving a new cantilever response function $\chi'(\omega)$.

$$\chi'(\omega) = \frac{\chi(\omega)}{1 \pm C\chi(\omega)} \tag{7}$$

The sign is $\pm$ is for a negative or a positive feedback loop control, respectively. The cantilever response can therefore be changed as long as it is feasible to perform the corresponding feedback loop (Koralek et al., 2000; Liang et al., 2000). Thus the low quality factor Q of the cantilever in a liquid can be increased to a value Q_{eff} by using a controller

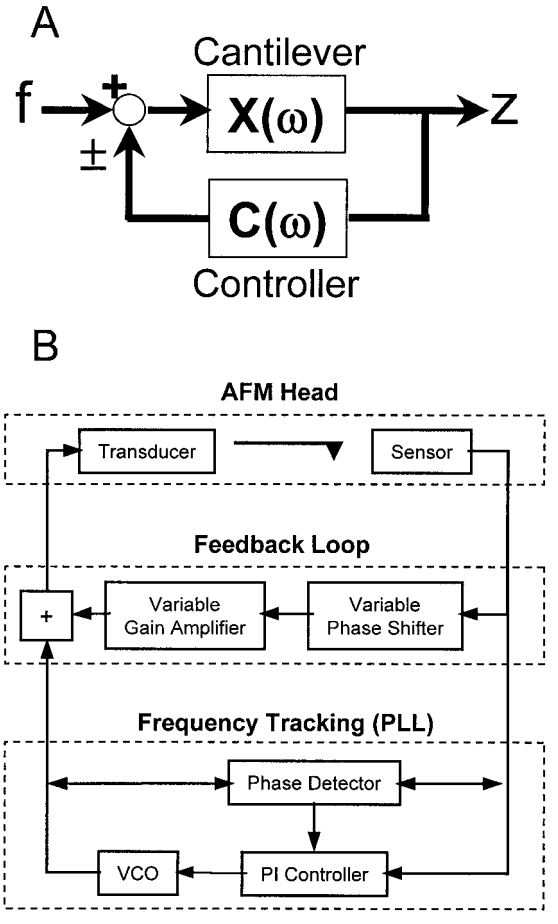

FIGURE 2 (*A*) Scheme of the cantilever motion control. (*B*) Diagram of the technique to increase the quality factor of the cantilever in liquid.

transfer function (Tamayo et al., 2000; Humphris et al., 2000):

$$C(\omega) = i\frac{\omega}{\omega_0}k\left(\frac{1}{Q} - \frac{1}{Q_{\text{eff}}}\right) \tag{8}$$

This frequency-dependent transfer function can be simplified by assuming that the driving frequency is very close to the resonant frequency of the cantilever. This approximation is particularly accurate for the high effective quality factors used in this technique.

$$C(\omega) = ik\left(\frac{1}{Q} - \frac{1}{Q_{\text{eff}/}}\right) = e^{i\pi/2} \times G \tag{9}$$

This controller can be performed with a positive feedback loop that consists of a variable phase shifter and a variable gain amplifier. Fig. 2 *B* shows a schematic of the experimental set-up. The positive feedback loop monitors the response of the cantilever detected by the sensor element, composed of the photodiode detector and a lock-in amplifier, giving a signal proportional to the main harmonic of the cantilever oscillation $z_1(\omega) = A_1 e^{i(\omega t - \varphi)}$. This signal is shifted 90° by the variable phase shifter, amplified with a gain G by the variable gain amplifier, and the processed signal is added to the driving signal of the cantilever. In other words, the cantilever is excited by two forces, the standard driving force $F_{\text{ext1}} = F_0\, e^{i\omega t}$ and a cantilever motion-dependent force $F_{\text{ext2}} = Ge^{i\pi/2}A_1 e^{i(\omega t - \varphi)}$. Thus the motion of the cantilever can be described by the differential equation of a damped harmonic oscillator driven by $F_{\text{ext1}} + F_{\text{ext2}}$:

$$m\frac{d^2z}{dt^2} + \gamma\frac{dz}{dt} + kz = F_0 e^{i\omega t} + Ge^{i\pi/2}A_1 e^{i(\omega t - \varphi)} + F_{\text{int}}(z) \tag{10}$$

where m is the effective mass of the cantilever and γ is the damping constant of the system due to the hydrodynamic damping between the cantilever and the environment and the internal friction of the cantilever. As long as the cantilever oscillation is sinusoidal, $z = z_1(\omega)$, the velocity of the cantilever can be expressed as

$$\frac{dz}{dt} = i\omega A_1 e^{i(\omega t - \varphi)} = \omega e^{i\pi/2} z, \tag{11}$$

and Eq. 10 can be written as:

$$m\frac{d^2z}{dt^2} + \gamma\frac{dz}{dt} + kz = F_0 e^{i\omega t} + \frac{G}{\omega}\frac{dz}{dt} \tag{12}$$

which produces:

$$m\frac{d^2z}{dt^2} + \gamma_{\text{eff}}\frac{dz}{dt} + kz = F_0 e^{i\omega t} \tag{13}$$

and

$$\gamma_{\text{eff}} = \gamma - \frac{G}{\omega} \tag{14}$$

γ_{eff} is the effective damping constant resulting from the positive feedback loop and can be increased or reduced (Sulchek et al., 2000), changing the quality factor according to the relation $Q_{\text{eff}} = m\omega_0/\gamma_{\text{eff}}$. This set-up is valid for a sinusoidal cantilever motion as that in the absence of tip-sample interaction or in DFM with high Q, as those found in air, gas, or vacuum. In the DFM in liquid, the cantilever motion is not sinusoidal, it is composed of a significant contribution of higher harmonics as it was shown above. In the rest of this work this point will be reminded and discussed, proving that a more complex experimental set-up is not necessary.

The experimental set-up (Fig. 2 *B*) also includes a phase-locked loop (PLL) to track the resonant frequency of the system. This is optional, but improves the performance of the microscope. The PLL produces a driving signal of the form $F_{\text{ext1}}(t) = F_0 e^{i\omega t}$ and monitors the cantilever response, adjusting the driving frequency, $\omega = 2\pi f$, to maintain a phase difference of 90° compared to the driving signal, i.e., maintaining the system at resonance. The PLL permits the determination of the elastic and dissipative components of the tip-sample interaction by measuring the resonant frequency and the amplitude at resonance. This is particularly advantageous for single molecule force spectroscopy (Humphris et al., 2000), but it can also be critical for imaging, as will be shown.

Cantilever response in liquid with *Q*-control

One deviation from the behavior of a damped harmonic oscillator is that the effective damping depends on the frequency (Eq. 14). However, γ_{eff} is constant when the microscope works at a single frequency. It can also be approximated to a constant when the resonance is tracked by the phase-locked loop, as the resonant frequency shifts are typically between two and three orders of magnitude smaller than the resonant frequency. Fig. 3 *A* shows a simulation of the response for a cantilever with a naturally high Q of 100 (*line*) and for a cantilever with a natural Q of 2 increased to an effective value of 100 by the Q-control (*circles*). The amplitude and the phase shift only show a significant deviation when the frequency is far from resonance.

Fig. 3 *B* shows the experimental response of a cantilever in aqueous solution driven by mechanical-acoustic excitation (*gray line*). The frequency spectrum is a convolution of the resonances of the fluid cell, cantilever base, liquid, and cantilever (Lantz et al., 1999). A direct excitation of the cantilever is required to isolate the cantilever response. This is performed by using an AC magnetic field to excite magnetically coated cantilevers (Han et al., 1996) (Fig. 3 *B*, *black line*). The broad peak corresponds to a very low quality factor of 2-3. Fig. 3 *C* shows the cantilever response with Q-control using magnetic excitation, for an effective Q of ~270.

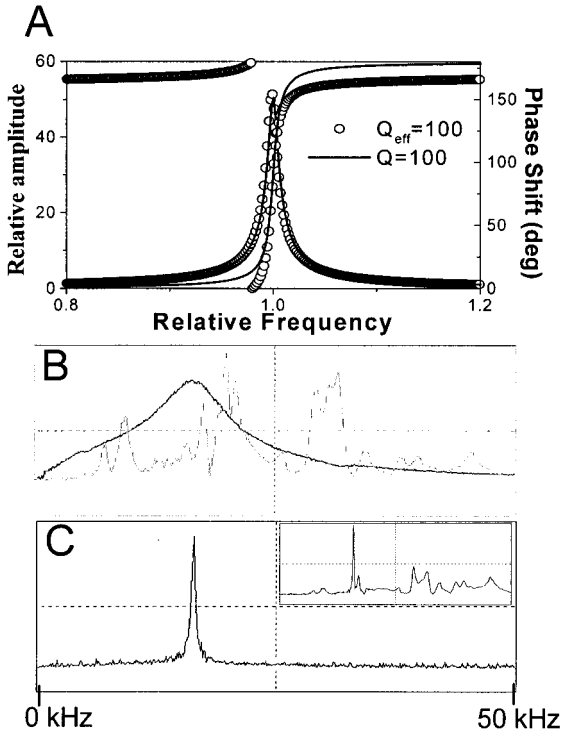

FIGURE 3 (*A*) Simulation of the amplitude and phase response for a cantilever with a natural quality factor of 100 (*line*), and for a cantilever with a natural quality factor of 2 increased to an effective Q of 100 by Q-control (*circles*). (*B*) Experimental frequency spectrum of a cantilever (k = 0.37 N/m) in aqueous solution driven by mechanical-acoustic excitation (*gray trace*) and by magnetic excitation (*black trace*). (*C*) Experimental frequency spectrum of the same cantilever as in (*B*) by using the Q-control ($Q_{\text{eff}} \approx 270$), driven by magnetic and mechanical-acoustic (*inset*) excitation methods.

Effective Q values of ~1000 can be reached, about three orders of magnitude higher than the natural Q value of the cantilever in fluid. However, very high effective Q values are unstable for imaging. For an ideal operation of the Q-control device, the highest Q value is limited by the changes of the liquid viscosity as a consequence of thermal fluctuations. For gains $G > \gamma\omega$, the effective damping constant is negative, and the cantilever oscillation is unstable (Eq. 14). Then, the maximum gain is $G = (\gamma - \Delta\gamma)\omega$, and the minimum effective damping factor is $\gamma_{\text{eff}} = \Delta\gamma$, where $\Delta\gamma$ is the damping factor variation as a consequence of the thermal fluctuations. For instance, the viscosity of pure water (~0.85 mPa s) changes ~2% as the temperature changes 1 K close to *RT*. Assuming 0.1 *K* fluctuations, the theoretical limit of the effective Q for standard cantilevers is ~1000.

Interestingly, the cantilever response can still be identified among the other resonances for mechanical-acoustic excitation (Fig. 3 *C*, *inset*). This can be explained as follows: in mechanical-acoustic excitation, the force is transmitted through the fluid cell and then either through the liquid or the cantilever base to the cantilever. The frequency spectrum is the product of the frequency-dependent transmission function of the excitation force and the cantilever response. For a very low Q, the frequency spectrum is dominated by the transmission function as consequence of the broad resonant peak of the cantilever. For a high Q, however, the narrow cantilever response filters the transmission function for frequencies out of resonance.

Fig. 4 *A* shows a simulation of a typical cantilever response with a resonant frequency of 12.5 kHz and $Q = 2$ (*dashed trace*, value in the range for short V-shaped cantilevers) and that through a resonance of the fluid cell, liquid, and cantilever base assembly at 9 KHz (*solid trace*) where the cantilever resonance cannot be observed. This curve shows a common situation in TM AFM in liquid using mechanical excitation, in which the frequency dependence of the transmission force dominates the cantilever response. In fact, one of the strongest resonances using mechanical acoustic excitation is located at 8-9 kHz, being one of the frequencies most used in TM AFM in liquid. Fig. 4 *B* shows the frequency spectrum for mechanical-acoustic excitation when Q-control is used to reach $Q_{\text{eff}} = 100$. To increase the effective quality factor, the variable phase shifter is manually adjusted to 90° to compensate for the phase lag of a few degrees from the electronics. During the tuning, the frequency spectrum shows an evolution of the cantilever resonance peak and excitation force transmission peak. The

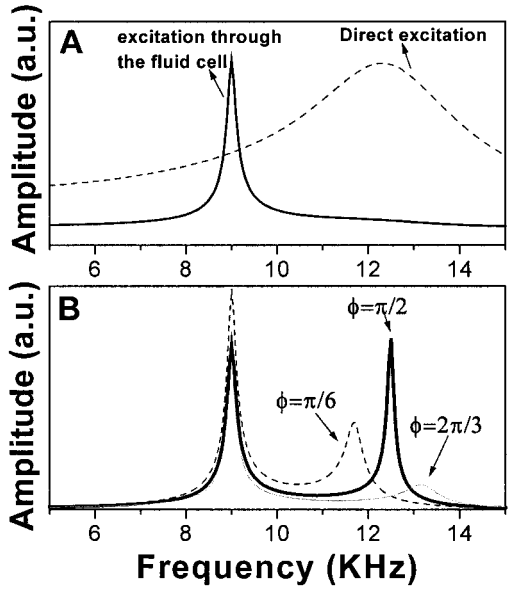

FIGURE 4 (*A*) Simulation of the frequency spectrum of a cantilever in liquid by using direct excitation (*dashed line*) and by excitation of the fluid cell (*solid line*). (*B*) Scheme of the identification of the cantilever resonance with Q-control using excitation of the fluid cell. The graph shows the frequency spectrum for different phase shifts ϕ of the variable phase shifter. The effective quality factor is 100 when $\phi = \pi/2$.

adjustment of the variable phase shifter produces a shifting of the cantilever peak and a change in its height. However, this only changes the amplitude of the excitation force transmission peak, not its frequency position. Therefore, the cantilever peak is identified as the shifting peak, and a phase shift of 90° is reached when the height of this peak is maximized.

FORCES

Fig. 5 shows numerical calculations of the maximum force on the sample (*A*), the maximum indentation depth (*B*), and the tip-sample contact time (*C*), all per oscillation cycle, as a function of the natural quality factor in TM AFM (*triangles*). The spring constant is 0.4 N/m, the free amplitude is 10 nm, the damped/free amplitude ratio is 0.9, the tip radius is 50 nm, and the elastic modulus of the sample is 1 GPa, close to that of some proteins. The logarithm of the force decreases approximately linearly with the logarithm of *Q*.

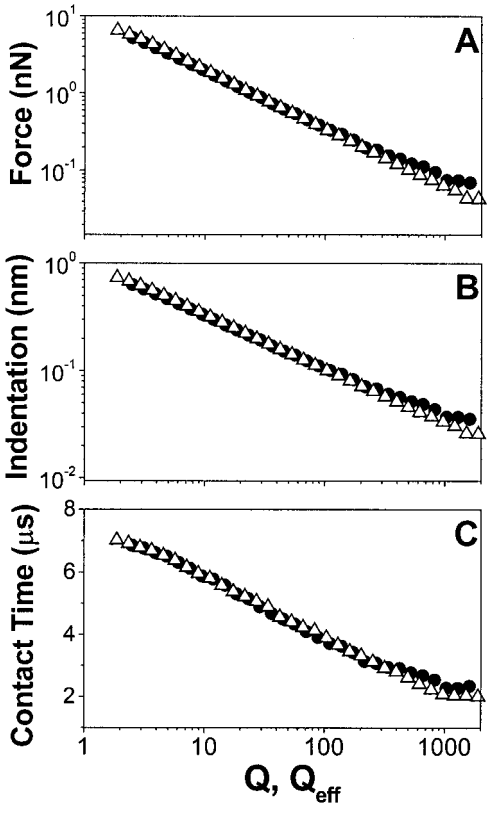

FIGURE 5 Numerical simulations of the force (*A*), indentation depth (*B*), and tip-sample contact time (*C*) in TM AFM as a function of the quality factor (*triangles*), and as a function of the effective quality factor by using *Q*-control (*circles*) for a cantilever with a natural quality factor of 1.5. The spring constant is 0.4 N/m, the free amplitude is 10 nm, the damped/free amplitude ratio is 0.9, the tip radius is 50 nm, and the elastic modulus of the sample is 1 GPa. The driving frequency is equal to the resonance, f_0 = 12.5 kHz. The values of the force and indentation depth are the maximum values per oscillation cycle.

More interestingly, the forces for the low quality factors found in liquids ($Q \approx 1$–3) can be as high as 10 nN, producing a tip indentation into the sample of up to 1 nm that would distort the structure of the biomolecules. The lateral spatial resolution can be estimated from the diameter of the contact between the tip and the sample during the contact. Applying the Hertz model (Israelachvili, 1992), the diameter of the contact corresponding to a deformation d = 0.7 nm and a tip radius R = 50 nm is $2(Rd)^{1/2} \approx 12$ nm. Subnanometer spatial resolution can only be achieved with a quality factor of several hundreds. Moreover, a higher Q value produces a smaller contact time between the tip and the sample (Fig. 5 *C*).

To determine the tip-sample interaction in TM AFM with the *Q*-control technique described above, the differential equation 2 is solved numerically (see Materials and Methods). The *Q*-control used here assumes a sinusoidal cantilever motion to increase to the quality factor. However, in TM AFM in liquids the cantilever motion is significantly anharmonic (Chen et al., 1996; Tamayo, 1999), so the cantilever response with an effective quality factor can differ from that with a real quality factor of the same value. Fig. 5 shows the calculations of the force, indentation depth, and contact time as a function of the effective quality factor (Q_{eff}) for a cantilever with a natural Q value of 1.5 (*solid circles*). These results are very similar to those of a cantilever with a natural Q of the same value (*triangles*), showing only a small deviation at very high Q values.

Fig. 6 shows measurements of the cantilever amplitude and tip-sample average force as a function of the cantilever position for the standard TM AFM technique and for TM AFM with *Q*-control. The measurements were performed on mica in PBS buffer solution. The average force per oscillation cycle is deduced by integrating the differential equation of the motion (Eq. 1) during an oscillation cycle. Most of the terms average zero, leading to:

$$k\langle z\rangle = \oint F_{\text{int}}(z)dz \tag{15}$$

Thus the average deflection $\langle z\rangle$ of the cantilever (experimental magnitude) multiplied by the spring constant gives the average tip-sample interaction force. Without *Q*-control, the average force between the tip and the sample exhibits an increasing positive value as soon as the amplitude is damped (Fig. 6, *A* and *B*). Average forces of several nanonewtons are produced in TM AFM in liquids. However, the average force is dramatically reduced to ~100 pN with the use of the *Q*-control for an effective Q value of ~410 (Fig. 6, *C* and *D*). Another remarkable difference is that the damped amplitude decreases with a slope of ~1/3 as the cantilever approaches the sample (Fig. 6 *B*), while this slope is ~1 with *Q*-control as it occurs in air (Fig. 6 *D*).

For high effective Q values, the amplitude is significantly damped before the intermittent contact regime is reached

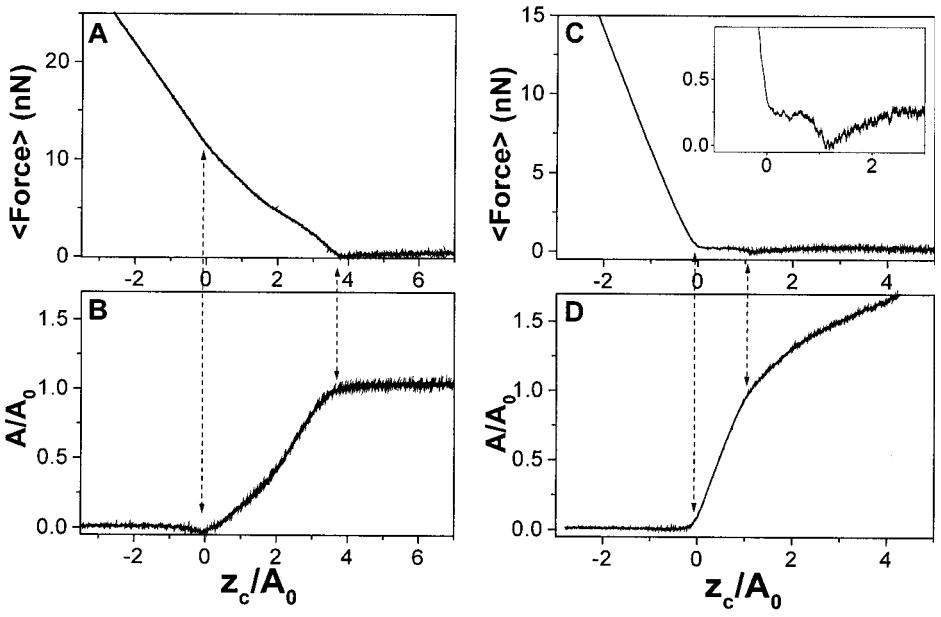

FIGURE 6 Experimental curves of the average tip-sample force as a function of the cantilever position for conventional TM AFM in liquid (*A*) and for TM AFM in liquid with *Q*-control (*C*). (*B*) and (*D*) show the simultaneously acquired curves of the amplitude with no *Q*-control and with *Q*-control, respectively. The cantilever position has been divided by the free amplitude (10-15 nm) near the sample to ease the comparison. The spring constant is 0.37 N/m, the liquid is PBS buffer, and the sample is mica. The effective quality factor of the cantilever with *Q*-control is ~410 at 400 nm away from the mica sample.

(Fig. 6 *D*). In this situation the cantilever oscillation is very sensitive to the increase of the hydrodynamic damping as the cantilever approaches the sample in the micron range. Thus the effective Q value of the cantilever increases by a factor of ~2 as the cantilever retracts 400 nm from near surface.

SPECTROSCOPY

In TM AFM in air, the measurement of the phase lag of the cantilever oscillation with respect to the excitation force has been used to map compositional variations with high sensitivity. Numerical calculations have shown that the phase contrast arises from variations in the energy dissipated between the tip and the sample due to nonconservative interactions (Tamayo and García, 1997). This is because the cantilever motion is sinusoidal in the intermittent contact regime for high quality factors ($Q > 10$), such as in air ($Q \approx$ 50-500). Hence the relationship between the phase shift and the energy dissipated per oscillation cycle can be determined by equating the external energy supplied by the driving force to the energy dissipated by the cantilever (Cleveland et al., 1998; Tamayo and García, 1998). The energy dissipated is split into two terms, one due to the hydrodynamic interaction between the cantilever and the environment and the other due to the energy dissipated between the tip and the sample. This leads to the following analytical relationship for DFM in gas or vacuum:

$$\sin \varphi = \frac{\omega}{\omega_0}\frac{A}{A_0} + \frac{QE_{\text{diss}}}{\pi k A A_0} \qquad (16)$$

where ω and ω_0 are, respectively, the driving and resonant frequencies, A is the damped amplitude and A_0 is the free amplitude at resonance, and E_{diss} is the energy dissipated between the tip and the sample per oscillation cycle. For low Q TM AFM, however, the phase contrast is reduced and the cantilever oscillation is not sinusoidal, consisting of an important contribution of higher harmonics, making Eq. 16 invalid and the interpretation of the phase contrast more complex (Tamayo, 1999).

Fig. 7 shows the contribution of the second harmonic to the cantilever oscillation as a function of the damped/free amplitude ratio. In conventional TM AFM in liquid, this contribution is very significant (*triangles*), but it is greatly reduced as the effective quality factor is increased by the *Q*-control (*circles*). Note that the technique presented here

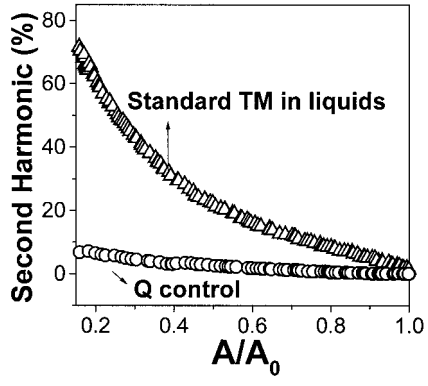

FIGURE 7 Experimental curves of the second harmonic contribution to the cantilever oscillation in TM AFM in liquid as a function of the damped/free amplitudes ratio without *Q*-control (*triangles*) and with *Q*-control (*circles*). The spring constant is 0.37 N/m, the liquid is PBS buffer, and the sample is mica. The effective quality factor of the cantilever with *Q*-control is ~400 at 400 nm away from the mica sample. Free amplitude is ~15-20 nm.

assumes a sinusoidal cantilever oscillation to increase the quality factor. For an oscillator motion composed of several frequency components as it occurs in DFM in liquid, the set-up should introduce an equivalent number of lock-in amplifiers to obtain a signal resulting from the feedback control proportional to the oscillator velocity. The results presented in Fig. 7 show that this complication can be avoided, as the cantilever response is that expected from a naturally high Q situation.

Relationship between energy dissipation and phase and resonant frequency shifts

To obtain the relationship between the phase shift and the energy dissipated in TM AFM in liquid with Q-control, the energy balance described above has to be performed, i.e., the external energy supplied to the cantilever is equated to the energy dissipated. In this technique, the external energy supplied to the cantilever has an additional term, E_{ext2} (see Eq. 10), then:

$$E_{ext} = E_{ext1} + E_{ext2}$$

$$= \oint (F_0 e^{i\omega t} + G e^{i\pi/2} A_1 e^{i(\omega t - \varphi)}) \frac{dz}{dt} dt \qquad (17)$$

This energy is equal to the energy dissipated by the cantilever (E_{cant}):

$$E_{cant} = \frac{m\omega_0}{Q} \oint \left(\frac{dz}{dt}\right)^2 dt + E_{diss} \qquad (18)$$

where the first term is the energy dissipated due to the hydrodynamic interaction between the cantilever and the liquid (E_h) and the second term is the energy dissipated between the tip and the sample per oscillation cycle. As the cantilever oscillation is approximately sinusoidal ($z \approx A_1 e^{i(\omega t - \varphi)} \equiv A e^{i(\omega - \varphi)}$) as shown in Fig. 7, this energy balance ($E_{ext1} + E_{ext2} = E_h + E_{diss}$) leads to:

$$\pi F_0 A \sin\varphi - \pi G A^2 = \frac{\pi k \omega / \omega_0}{Q} A^2 + E_{diss} \qquad (19)$$

For driving frequencies close to the resonant frequency:

$$\sin\varphi \cong \frac{A}{A_0} - \frac{Q_{eff} E_{diss}}{\pi k A A_0} \qquad (20)$$

where A_0 is the free amplitude at resonance.

Equation 20 is the same relationship as for DFM with high Q (Eq. 16). The phase contrast comes from variations in the nonconservative interactions between the tip and the sample, and this contrast is amplified by the effective quality factor (Q_{eff}). This is valid if the feedback keeps the damped amplitude A constant. This analytical relationship permits the transformation of the phase shift images into energy dissipation maps and can be particularly useful in the application of this technique to mapping receptors in cell membranes with the use of ligand-functionalized tips (Raab et al., 1999).

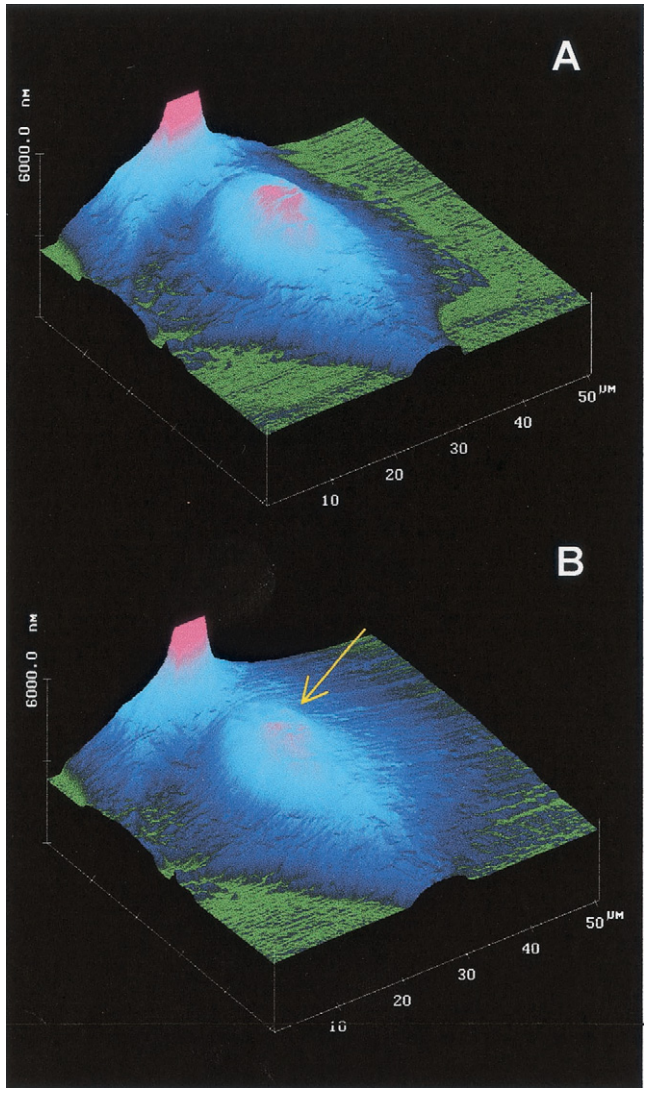

FIGURE 8 Height images of living rat kidney cells in liquid solution by using conventional TM AFM (A) and by using TM AFM with Q-control with an effective Q of ~300. Scan size is 50 × 50 μm^2. (B) The arrow indicates the region in which the images shown in Fig. 9 were acquired. The maximum height of the cells is ~2.5 μm.

In an alternative set-up, the resonant frequency and the amplitude at resonance are measured instead of the amplitude and phase shift at a fixed frequency. This is performed by using the phase-locked loop described above, which keeps $\sin\varphi = 1$ in Eq. 20. In this technique, the amplitude at resonance is kept constant to obtain the topography, and the shift of the resonant frequency is measured to map the compositional variations of inhomogeneous surfaces. In this way the dissipative and the elastic interactions are decoupled. The topography corresponds to contours of equal

energy dissipation and the frequency signal maps the elastic interaction.

IMAGING

In this section, high-Q dynamic force microscopy is applied to visualize living rat kidney (NRK) cells (Henderson, 1994; Kuznetsov et al., 1997; LeGrimellec et al., 1998; Vie et al., 2000; Ohnesorge et al., 1997; Radmacher et al., 1992; Kasas et al., 1997). Fig. 8 *A* shows the height image of a cell using the standard tapping mode technique in liquid. This image does not significantly differ from the topography acquired with Q-control, in which the quality factor is increased by two orders of magnitude (Fig. 8 *B*). This is due to the large height of the cell that dominates over smaller height variations associated to the complex structure of the cell. However, the phase images, which are independent of the topography, exhibit a dramatic difference; Fig. 9, *A* and *B* show the corresponding phase shift images of the central region of the cell without Q-control and with Q-control, respectively (phase range 70°). Q-control produces a significant enhancement of the phase contrast and of the spatial resolution. First, the phase shift image exhibits a larger contrast between the nucleus and the rest of the cell, and between components in the nuclear region. Second, this image shows a filamentous network with substantially higher resolution, and also reveals fine details not visible without Q-control, particularly over the nuclear region. This is better observed by applying a contrast enhancement routine (see details in Materials and Methods) to the images that eases the visualization of fine details (Fig. 9, *C* and *D*). The filamentous network visible in the phase shift image is attributed to the structure of the submembranous cytoskeleton (Hoh and Schoenenberger, 1994; Vie et al., 2000).

The hydrodynamic damping significantly influences the tapping mode operation with the Q-control. The hydrodynamic damping increases as the cantilever approaches the sample (see Fig. 6 and related text), producing a decrease of the quality factor and a shift of the resonance to lower frequencies as the effective mass increases. Although the decrease of Q can be compensated by increasing the gain of the variable gain amplifier during imaging, the shift of the resonant frequency makes tuning the cantilever at distance of ~500-1000 nm necessary to prevent a shift larger than the very small line width of the resonance peak ($\Delta f \approx f_0/Q \sim 10$ Hz). The tuning of the cantilever at a small distance can be unstable as a consequence of undesirable contacts between the tip and the sample in very rough

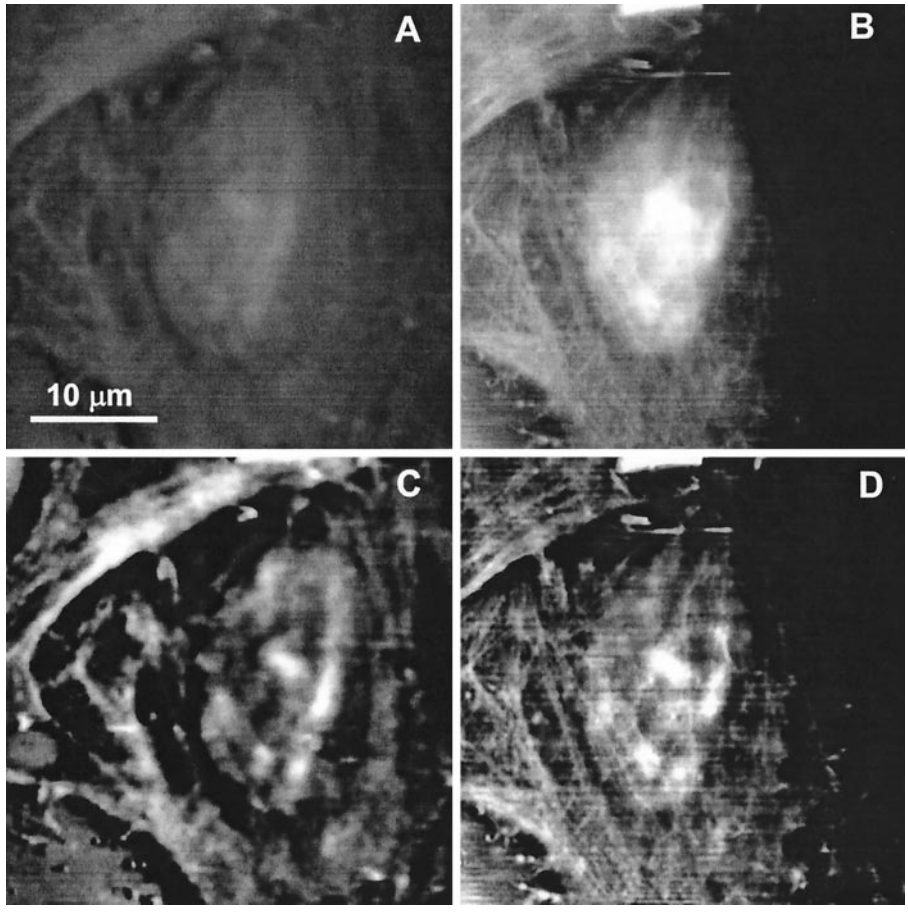

FIGURE 9 Phase shift images of the central region of the rat kidney cell indicated with an arrow in Fig. 8 without Q-control (*A*) and with Q-control (*B*) with a phase range of 70°. (*C*) and (*D*) are (*A*) and (*B*) images processed to highlight the cell membrane structure at high resolution. Scan size is $36 \times 36\ \mu m^2$.

samples, such as cells. To overcome this problem, we combine the *Q*-control unit with a phase-locked loop unit to track the resonant frequency. Thus, the amplitude at resonance and the resonant frequency shift are measured instead of the amplitude and phase shift. The amplitude at resonance is kept constant by the feedback to provide the topography of the sample and the frequency signal is used to map compositional variations on the surface.

Fig. 10, *A* and *B* show the topography and frequency images of a living cell using the alternative set-up described above. The resonant frequency shift image exhibits a remarkable contrast between the cell and the substrate (200-210 Hz) and between intracellular components (≈5 Hz).

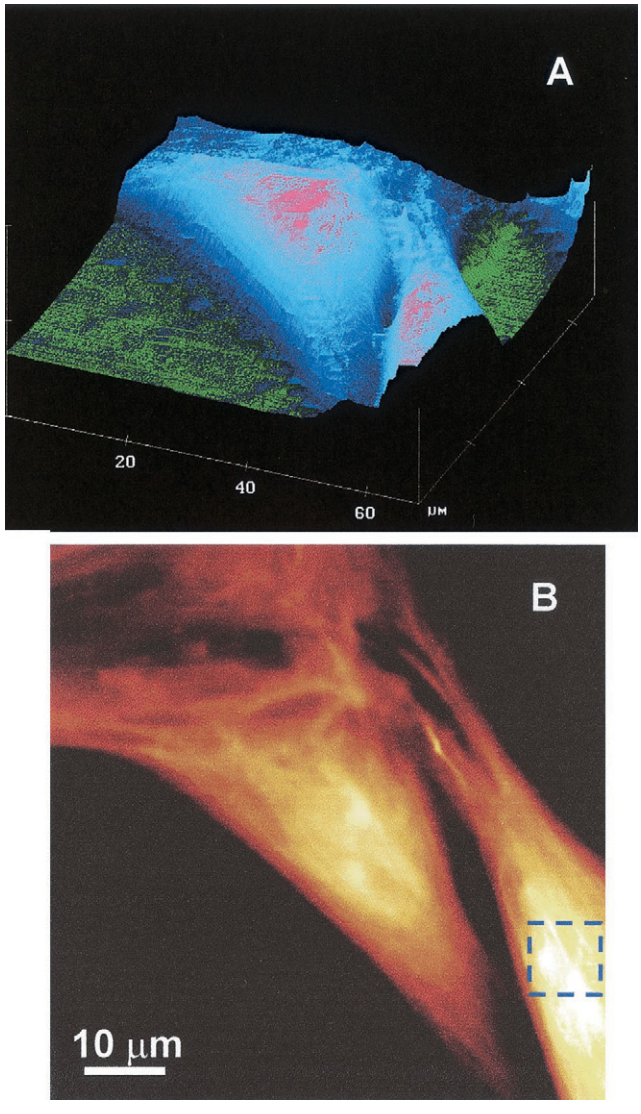

FIGURE 10 (*A*) Height image of a living rat kidney cell in liquid solution by using *Q*-control and tracking the resonant frequency. The maximum height of the cell is ~2.2 μm. (*B*) Corresponding resonant frequency shift image. The frequency range is 200 Hz. The effective *Q* is ~300 and the scan size is 68 × 68 μm^2. The square marked in (*B*) was imaged at higher resolution, and it is shown in Fig. 11.

Fig. 11 *A* shows a smaller frequency image (*dashed square* in Fig. 10 *B*), which reveals a well-defined structure of fibers. The phase shift image without *Q*-control of the same region shows lower resolution and lower signal/noise ratio (Fig. 11 *B*). The distribution of the fibers is also distorted, probably due to the high forces between the tip and the sample in standard tapping mode in liquids. The enhancement of the spatial resolution can be also seen in the corresponding profiles along the same scan line (Fig. 11, *C* and *D*).

The most accepted mechanism responsible for the height images of living cells is the deformation of the very soft plasma membrane around the intracellular structures (Hoh and Schoenenberger, 1994; Hassan et al., 1998). The very low Young's modulus of the cells (~10 kPa) suggests that the plasma membrane behaves as being transparent to the AFM tip; in fact, it has been reported that 1-10 pN results in a 1 nm deformation of the plasma membrane, so the height images reflect the stiffness of intracellular structures. The tip-sample force determines the depth of the observed intracellular structures within the cell. Thus, to characterize the submembranous intracellular structures at high resolution, such as the cytoskeleton fibers shown above, very low forces of a few tens of piconewtons are required, as those obtained with the technique described here. The lateral resolution is determined by the contact point between the tip and the object. Taking into account that the tip is a pyramid with a semi-angle of 35°, the resolution of the submembranous structure decreases linearly with the indentation depth. This explains the improvement of the resolution obtained above when the force goes from several nanonewtons (conventional TM AFM) where the tip indents the plasma membrane >500 nm, to a few tens of piconewtons, producing an indentation depth of ~1-10 nm (high-*Q* DFM).

The frequency contrast arises from variations in the elastic interaction between the tip and the sample. It is tempting to relate this variation to the local elastic modulus of the surface. However, Fig. 10 *B* shows a higher frequency shift over the cell (which is very soft) than over the glass substrate (which is hard), in contrast to the expected behavior where the resonant frequency should shift to higher values over stiffer regions. However, the tip-sample interaction in liquids is more complex. It is quite possible that the tip never touches the sample during the oscillation with the low forces of several tens of piconewtons used with this technique. The elastic interaction should be very sensitive to the properties of the liquid confined between the tip and the sample (Lantz et al., 1999). Indeed, when a liquid is confined in a narrow gap a new dynamic behavior emerges in which the viscosity increases several orders of magnitude in the nanometer regime and the liquid solidifies for gaps of a few molecular layers (Granick, 1991). Therefore, a major theoretical understanding of the relationship between the physical properties of the confined liquid and those of the boundaries (tip and sample) is necessary to understand the

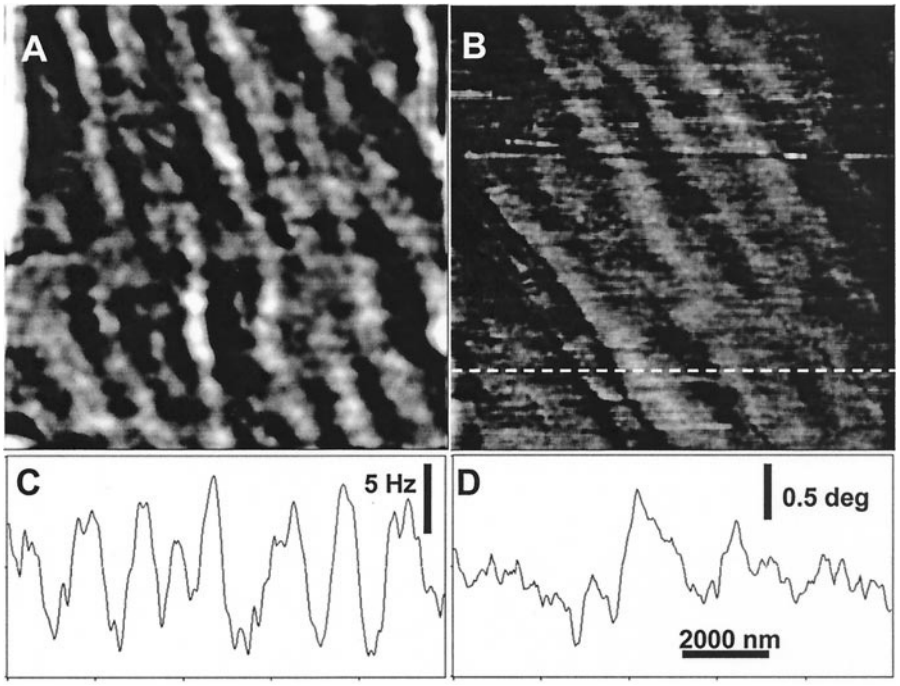

FIGURE 11 (*A*) Resonant frequency image of the region marked in Fig. 10 *B* by using *Q*-control. (*B*) Phase shift image of the same region with conventional TM AFM in liquid. (*C*) and (*D*) are the profiles along the same scan line in (*A*) and (*B*), respectively. The scan line is marked in (*B*) with a dashed line. Scan size is $10 \times 10\ \mu m^2$.

origin of the nonconservative (phase contrast) and conservative interactions (frequency contrast) between the tip and the sample in high-*Q* DFM in liquid.

CONCLUSIONS

Here we have presented a new dynamic force microscopy technique in liquid in which the low quality factor of the cantilever can be increased up to three orders of magnitude by implementing a positive feedback. The combination of the positive feedback and phase-locked loop unit to track the resonant frequency allows imaging with forces smaller than 100 pN, about two orders of magnitude lower than the forces in the conventional tapping mode technique. Moreover, either the phase shift or resonant frequency can be measured to provide a compositional map of the surface with high sensitivity and high spatial resolution. In the piconewton force regime new interactions must be considered, in particular the role of the confined liquid between the tip and the sample, and the increase of the hydrodynamic damping as the cantilever approaches the sample at distances smaller than a few microns. This will require new theoretical models and specific instrumentation. Once these difficulties are overcome, this technique will provide the best AFM images of biomolecules and will make the atomic force microscope a technique for single molecule force spectroscopy with a sensitivity comparable to other techniques, such as optical tweezers.

REFERENCES

Anczykowski, B., J. P. Cleveland, D. Krüger, V. Elings, and H. Fuchs. 1998. Analysis of the interaction mechanisms in dynamic mode SFM by means of experimental data and computer simulation. *Appl. Phys. A.* 66:S885–S889.

Binnig, G., C. F. Quate, and Ch. Gerber. 1986. Atomic force microscopy. *Phys. Rev. Lett.* 56:930–933.

Bustamante, C., and D. Keller. 1995. Scanning force microscopy in biology. *Phys. Today.* 32:32–38.

Butt, H. J., P. Siedle, K. Seifert, K. Fendler, T. Seeger, E. Bamberg, A. L. Weisenhorn, K. Goldie, and A. Engel. 1993. Scan speed limit in atomic force microscopy. *J. Microsc.* 169:75–84.

Chen, G. Y., R. J. Warmack, P. I. Oden, and T. Thundat. 1996. Transient response of tapping scanning force microscopy in liquids. *J. Vac. Sci. Technol. B.* 14:1313–1317.

Chen, G. Y., R. J. Warmack, T. Thundat, D. P. Allison, and A. Huang. 1994a. Resonance response of scanning force microscopy cantilevers. *Rev. Sci. Instrum.* 65:2532–2537.

Chen, J., R. K. Workman, D. Sarid, and R. Hoper. 1994b. Numerical simulations of a scanning force microscope with a large-amplitude vibrating cantilever. *Nanotechnology.* 5:199–204.

Cleveland, J. P., B. Anczykowski, A. E. Schmid, and V. B. Elings. 1998. Energy dissipation in tapping-mode atomic force microscopy. *Appl. Phys. Lett.* 72:2613–2615.

Durig, U., H. R. Steinauer, and N. Blanc. 1997. Dynamic force microscopy by means of the phase-controlled oscillator method. *J. Appl. Phys.* 82:3641–3651.

Engel, A., Y. Lyubchenko, and D. Müller. 1999. Atomic force microscopy: a powerful tool to observe biomolecules at work. *Trends Cell Biol.* 9:77–80.

Garbini, J. L., K. J. Bruland, W. M. Dougherty, and J. A. Sidles. 1996. Optimal control of force microscope cantilevers. 1. Controller design. *J. Appl. Phys.* 80:1951–1958.

Giessibl, F. J. 1995. Atomic-resolution of the silicon (111) − (7 × 7) surface by atomic force microscopy. *Science.* 267:68–71.

Granick, S. 1991. Motions and relaxations of confined liquids. *Science.* 253:1374–1379.

Hansma, P. K., J. P. Cleveland, M. Radmacher, D. A. Walters, P. E. Hillner, M. Bezanilla, M. Fritz, D. Vie, H. G. Hansma, C. B. Prater, J. Massie, L. Fukunaga, J. Gurley, and V. Elings. 1994. Tapping mode atomic-force microscopy in liquids. *Appl. Phys. Lett.* 64:1738–1740.

Han, W., S. M. Lindsay, and T. Jing. 1996. A magnetically driven oscillating probe microscope for operation in liquids. *Appl. Phys. Lett.* 69:4111–4113.

Hassan, E. A., W. F. Heinz, M. D. Antonik, N. P. D'Costa, S. Nageswaran, C. A. Schoenenberger, and J. H. Hoh. 1998. Relative microelastic mapping of living cells by atomic force microscopy. *Biopys. J.* 74: 1564–1578.

Henderson, E. 1994. Imaging of living cells by atomic force microscopy. *Progr. Surf. Sci.* 46:39–60.

Hoh, J. H., and C. A. Schoenenberger. 1994. Surface morphology and mechanical properties of MDCK monolayers by atomic force microscopy. *J. Cell Sci.* 107:1105–1114.

Humphris, A. D. L., J. Tamayo, and M. J. Miles. 2000. Active quality factor control in liquids for force spectroscopy. *Langmuir.* 16: 7891–7894.

Israelachvili, J. 1992. Intermolecular and surface forces, 2nd Ed. Academic Press, New York.

Kasas, S., N. H. Thomson, B. L. Smith, P. K. Hansma, J. Miklossy, and H. G. Hansma. 1997. Biological applications of the AFM: from single molecules to organs. *Int. J. Imaging Systems Technol.* 8:151–161.

Koralek, D. O., W. F. Heinz, M. D. Antonik, A. Baik, and J. H. Hoh. 2000. Probing deep interaction potentials with white-noise-driven atomic force microscopy cantilevers. *Appl. Phys. Lett.* 76:2952–2954.

Kuznetsov, Y. G., A. J. Malkin, and A. McPherson. 1997. Atomic force microscopy studies of living cells: visualization of motility, division, aggregation, transformation, and apoptosis. *J. Struct. Biol.* 120: 180–191.

Lantz, M., Y. Z. Liu, X. D. Cui, H. Tokumoto, and S. M. Lindsay. 1999. Dynamic force microscopy in fluid. *Surface and Interface Analysis* 27:354–360.

LeGrimellec, C., E. Lesniewska, M. C. Giocondi, E. Finot, V. Vie, and J. P. Goudonnet. 1998. Imaging of the surface of living cells by low-force contact-mode atomic force microscopy. *Biophys. J.* 75:695–703.

Liang, S., D. Medich, D. M. Czajkowsky, S. Sheng, J.-Y. Yuan, and Z. Shao. 2000. Thermal noise reduction of mechanical oscillators by actively controlled external dissipative forces. *Ultramicroscopy.* 84: 119–125.

Martin, Y., C. C. Williams, and H. K. Wickramasinghe. 1987. Atomic force microscope force mapping and profiling on a sub 100-Å scale. *J. Appl. Phys.* 61:4723–4729.

Mertz, J., O. Marti, and J. Mlynek. 1993. Regulation of a microcantilever response by force feedback. *Appl. Phys. Lett.* 62:2344–2346.

Ohnesorge, F. M., J. K. H. Horber, W. Haberle, C. P. Czerny, D. P. E. Smith, and G. Binnig. 1997. AFM review study on pox viruses and living cells. *Biophys. J.* 73:2183–2194.

Putman, C. A. J., K. O. van der Werf, B. G. de Grooth, N. F. van Hulst, and J. Greve. 1994. Tapping mode atomic-force microscopy in liquid. *Appl. Phys. Lett.* 64:2454–2456.

Raab, A., W. H. Han, D. Badt, S. J. SmithGill, S. M. Lindsay, H. Schindler, and P. Hinterdorfer. 1999. Antibody recognition imaging by force microscopy. *Nat. Biotechnol.* 17:902–905.

Radmacher, M., R. W. Tillmann, M. Fritz, and H. E. Gaub. 1992. From molecules to cells—imaging soft materials with the atomic force microscope. *Science.* 257:1900–1905.

Rugar, D., and P. K. Hansma. 1990. Atomic force microscopy. *Phys. Today.* 43:23–30.

Shao, Z. F., J. Mou, D. M. Czajkowsky, J. Yang, and J. Y. Yuan. 1996. Biological atomic force microscopy: what is achieved and what is needed. *Adv. Phys.* 45:1–86.

Sugurawa, Y., M. Ohta, H. Ueyama, and S. Morita. 1995. Defect motion on an InP(110) surface observed with noncontact atomic-force microscopy. *Science.* 270:1646–1648.

Sulchek, T., R. Hsieh, J. D. Adams, G. G. Yaralioglu, S. C. Minne, C. F. Quate, J. P. Cleveland, A. Atalar, and D. M. Adderton. 2000. High-speed tapping mode imaging with active Q control for atomic force microscopy. *Appl. Phys. Lett.* 76:1473–1475.

Tamayo, J. 1999. Energy dissipation in tapping-mode scanning force microscopy with low quality factors. *Appl. Phys. Lett.* 75:3569–3571.

Tamayo, J., and R. Garcia. 1996. Deformation, contact time, and phase contrast in tapping mode scanning force microscopy. *Langmuir.* 12: 4430–4435.

Tamayo, J., and R. Garcia. 1997. Effects of elastic and inelastic interactions on phase contrast images in tapping-mode scanning force microscopy. *Appl. Phys. Lett.* 71:2394–2396.

Tamayo, J., and R. Garcia. 1998. Relationship between phase shift and energy dissipation in tapping-mode scanning force microscopy. *Appl. Phys. Lett.* 73:2926–2928.

Tamayo, J., A. D. L. Humphris, and M. J. Miles. 2000. Piconewton regime dynamic force microscopy in liquid. *Appl. Phys. Lett.* 77:582–584.

Vie, V., M.-C. Giocondi, E. Lesniewska, E. Finot, J.-P. Goudonnet, and C. Le Grimellec. 2000. Tapping-mode atomic force microscopy on intact cells: optimal adjustment of tapping conditions by using the deflection signal. *Ultramicroscopy.* 82:279–288.

Zhong, Q., D. Inniss, K. Kjoller, and V. B. Elings. 1993. Fractured polymer silica fiber surface studied by tapping mode atomic-force microscopy. *Surf. Sci.* 290:L688–L692.